

Production of Ξ^* resonances in Σ^- induced reactions at 345 GeV/c

The WA89 Collaboration

M.I. Adamovich⁸, Yu.A. Alexandrov^{8,a}, S.P. Baranov^{8,a}, D. Barberis³, M. Beck⁵, C. Bérat⁴, W. Beusch², M. Boss⁶, S. Brons^{5,b}, W. Brückner⁵, M. Buénerd⁴, C. Busch⁶, C. Büscher⁵, F. Charignon⁴, J. Chauvin⁴, E.A. Chudakov^{6,c}, U. Dersch⁵, F. Dropmann⁵, J. Engelfried^{6,d}, F. Faller^{6,e}, A. Fournier⁴, S.G. Gerassimov^{5,8,f}, M. Godbersen⁵, P. Grafström², Th. Haller⁵, M. Heidrich⁵, E. Hubbard⁵, R.B. Hurst³, K. Königsmann^{5,g}, I. Konorov^{5,8,f}, N. Keller⁶, K. Martens^{6,h}, Ph. Martin⁴, S. Masciocchi^{5,i}, R. Michaels^{5,c}, U. Müller⁷, H. Neeb⁵, D. Newbold¹, C. Newsom^j, S. Paul^{5,f}, J. Pochodzalla⁵, I. Potashnikova⁵, B. Povh⁵, R.D. Ransome^k, Z. Ren⁵, M. Rey-Campagnolle^{4,l}, G. Rosner⁷, L. Rossi³, H. Rudolph⁷, C. Scheel^m, L. Schmitt^{7,f}, H.-W. Siebert⁶, A. Simon^{6,g}, V.J. Smith^{1,n}, O. Thilmann⁶, A. Trombini⁵, E. Vesin⁴, B. Volkemer⁷, K. Vorwalter⁵, Th. Walcher⁷, G. Wälder⁶, R. Werding⁵, E. Wittmann⁵, and M.V. Zavertyaev^{8,a}

¹ University of Bristol, Bristol, United Kingdom

² CERN, CH-1211 Genève 23, Switzerland.

³ Genoa University/INFN, Dipt. di Fisica, I-16146 Genova, Italy.

⁴ Grenoble ISN, F-38026 Grenoble, France.

⁵ Max-Planck-Institut für Kernphysik, Postfach 103980, D-69029 Heidelberg, Germany.

⁶ Universität Heidelberg, Physikal. Inst., D-69120 Heidelberg Germany. ^o

⁷ Universität Mainz, Inst. für Kernphysik, D-55099 Mainz, Germany. ^o

⁸ Moscow Lebedev Physics Inst., RU-117924, Moscow, Russia.

the date of receipt and acceptance should be inserted later

^a supported by the Deutsche Forschungsgemeinschaft, contract number 436 RUS 113/465, and Russian Foundation for Basic Research under contract number RFFI 98-02-04096.

^b Now at TRIUMF, Vancouver, B.C., Canada V6T 2A3

^c Now at Thomas Jefferson Lab, Newport News, VA 23606, USA

^d Now at Instituto de Fisica, Universidad San Luis Potosi, S.L.P. 78240, Mexico

^e Now at Fraunhofer Institut für Solarenergiesysteme, D-79100 Freiburg, Germany

^f Now at Technische Universität München, Garching, Germany

^g Now at Fakultät für Physik, Universität Freiburg, Germany

^h Now at Department of Physics and Astronomy, SUNY at Stony Brook, NY 11794-3800, USA

ⁱ Now at Max-Planck-Institut für Physik, München, Germany

^j University of Iowa, Iowa City, IA 52242, USA

^k Rutgers University, Piscataway, NJ 08854, USA.

^l permanent address: CERN, CH-1211 Genève 23, Switzerland

^m NIKHEF, 1009 DB Amsterdam, The Netherlands

ⁿ supported by the UK PPARC

^o supported by the Bundesministerium für Bildung, Wissenschaft, Forschung und Technologie, Germany, under contract numbers 05 5HD15L, 06 HD524I and 06 MZ5265

Abstract. We report on a measurement of the differential and total cross sections of inclusive production of Ξ^* resonances in Σ^- - nucleus collisions at 345 GeV/c. The cross section for inclusive Ξ_{1530}^0 production is about a factor of 5 below that of Ξ_{1320}^- hyperons. The products of cross section and branching ratio for the observed channels $\Xi_{1690}^0 \rightarrow \Xi^- \pi^+$, $\Xi_{1820}^- \rightarrow \Xi_{1530}^0 \pi^-$ and $\Xi_{1950}^- \rightarrow \Xi_{1530}^0 \pi^-$ are lower by yet another order of magnitude. The Ξ_{1820}^- and Ξ_{1950}^- resonances show significantly harder x_F and p_t distributions than Ξ^- and Ξ_{1530}^0 hyperons. A comparison of the x_F -distribution to PYTHIA and QGSM predictions provides only a partial agreement.

1 Introduction

The production of the ground state hyperons and also of their antiparticles has been studied extensively in previous experiments, using neutron, protons and Ξ^- as beam particles with momenta ranging up to 600 GeV/c [1–8]. In a recent paper [9] we have reported cross sections for inclusive Ξ^- production by Σ^- and π^- of 345 GeV/c and by neutrons of 260 GeV/c mean beam momenta. These measurements confirmed the important role of the valence quark overlap between the beam projectile and the produced baryon at high x_F , the ‘leading particle effect’.

Only few data exist on the production of excited hyperon resonances in such beams [5, 10, 11]. In ref. [11] a different x_F behaviour for Ξ^0 and Ξ_{1530}^0 was reported. This difference between the octet and the decuplet baryons was nicely reproduced in terms of the quark-diquark cascade model [12]. Within that model this feature is related to the diquark structure of the incident and produced baryons.

Here we extend this study for the first time to orbitally excited baryons and present cross section measurements for Ξ_{1530}^0 , Ξ_{1690}^0 , Ξ_{1820}^- and Ξ_{1950}^- production by Σ^- of 345 GeV/c mean momentum. The results on the x_F -dependence of the cross sections and on the ratio of Ξ^* and Ξ^- production will contribute to a better understanding of the complex process of hadron production in hadron beams. Furthermore, these data may help to explore the role of higher resonances for the spectral distributions of multiply strange hyperons which have recently been suggested [13] as an important diagnostic tool for the early freeze-out stage in ultra-relativistic heavy ion collisions.

2 Hyperon beam and experimental apparatus

The hyperon beam was derived from an external proton beam of the CERN-SPS, hitting a hyperon production target placed 16 m upstream of the experimental target. Negative secondaries with a mean momentum of 345 GeV/c and a momentum spread $\sigma(p)/p \approx 9\%$ were selected in a magnetic channel. The production angles relative to the proton beam were smaller than 0.5 mrad. At the experimental target, the beam consisted of π^- , K^- , Σ^- and Ξ^- in the ratio 2.3 : 0.025 : 1 : 0.008. A transition radiation detector (TRD) made of 10 MWPCs interleaved with foam radiators allowed π^- suppression at the trigger level. Typically, about $1.8 \cdot 10^5$ Σ^- and $4.5 \cdot 10^5$ π^- were delivered to the target during one SPS-spill, which had an effective length of about 1.5 s. More details can be found in [14].

Particle	Mass	Width	σ_{Data}	σ_{MC}
$\Lambda \rightarrow p\pi^-$	1115.7 ± 0.1		1.93	1.62
$\Xi^- \rightarrow \Lambda\pi^-$	1321.0 ± 0.1		2.68	2.32
$\Omega^- \rightarrow \Lambda K^-$	1672.5 ± 0.9		2.4	2.1
Ξ_{1530}^0	1532.2 ± 0.5	9.1	3.7	3.2
Ξ_{1820}^-	1817 ± 3	23 ± 13		3.4
Ξ_{1950}^-	1955 ± 6	68 ± 22		3.4

Table 1. Mean reconstructed masses and widths of Λ^0 , Ξ^- , Ω^- , Ξ_{1530}^0 , Ξ_{1820}^- and Ξ_{1950}^- and mass resolutions from data and Monte Carlo. All numbers are given in units of MeV/c².

The experimental target consisted of one copper and three carbon blocks arranged in a row along the beam, with thicknesses corresponding to $0.026 \lambda_I$ and three times $0.0083 \lambda_I$, respectively. At the target, the beam had a width of 3 cm and a height of 1.7 cm. Microstrip detectors upstream and downstream of the target measured the tracks of the incoming beam particles and of the charged particles produced in the target blocks. The target was positioned 14 m upstream of the centre of the Omega spectrometer magnet [15] so that a free field decay region of 10 m length was provided for hyperon and K_S decays. Tracks of charged particles were measured inside the magnet and in the field-free regions upstream and downstream by MWPCs and drift chambers, with a total of 130 planes. The Omega magnet provided a field integral of 7.5 Tm, and the momentum resolution achieved was $\sigma(p)/p^2 \approx 10^{-4}$ (GeV/c)⁻¹.

Downstream of the spectrometer, a ring-imaging Cherenkov detector, an electromagnetic calorimeter and a hadron calorimeter were placed. They were not used in the analysis presented here.

The main trigger selected about 25% of all interactions, using multiplicities measured in microstrip counters upstream and downstream of the target, and in scintillator hodoscopes and MWPCs behind the Omega magnet. Correlations between hits in different detectors were used in the trigger to increase the fraction of events with high-momentum particles, thus reducing background from low-momentum decay-pions in the beam. In addition, a reduced sample of beam trigger events were recorded for calibration purposes. The results presented in this article are based on 100 million events recorded in 1993.

3 Event selection

In the following, we describe the event selection for the decays $\Xi_{1530}^0 \rightarrow \Xi^- \pi^+$ and $\Xi^- \rightarrow \Xi_{1530}^0 \pi^-$. Cuts imposed

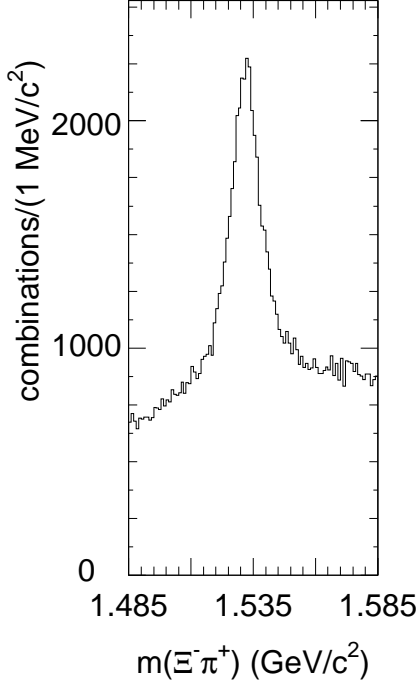


Fig. 1. Effective mass distribution of $\Xi^- \pi^+$ combinations.

on the data sample in this analysis are very similar to those used in the measurement of the Ξ^- production cross section [9] and in the search for $\Xi_{1690}^0 \rightarrow \Xi^- \pi^+$ decays [16].

First, Λ^0 candidates were reconstructed from all pairs of positive and negative tracks which formed a vertex downstream of the target. The minimum distance of approach between the tracks was required to be smaller than 5 mm. For each candidate the effective $p\pi^-$ mass and its error were calculated; the rms of the error was $\sigma_m \approx 2.2 \text{ MeV}/c^2$. The reconstructed $p\pi^-$ mass had to be within $\pm 15 \text{ MeV}/c^2$ around the known Λ^0 mass [17], the error of the mass determination was required to be less than $5 \cdot \sigma_m$.

Next, Ξ^- candidates were selected from all pairs of Λ^0 candidates and negative tracks which formed a vertex downstream of the target. Again the minimum distance of approach between the reconstructed Λ^0 track and the negative track was required to be smaller than 5 mm. A track corresponding to the Ξ^- track as reconstructed from the decay cascade had to be found in the microstrip detectors downstream of the target. This track was used in the reconstruction of the production vertex (see below). The effective $\Lambda\pi^-$ mass had to be within $\pm 15 \text{ MeV}/c^2$ of the Ξ^- mass, for the mass resolution a value of $\leq 5 \cdot \sigma_m$ was required, where $\sigma_m = 2.7 \text{ MeV}/c^2$ is the typical resolution.

Then, we required a production vertex containing at least one outgoing charged track in addition to the Ξ^- track. The reconstructed vertex position had to be within a target block. In each coordinate an additional margin of $3\text{-}\sigma$ was allowed. The transverse distance between the Σ^-

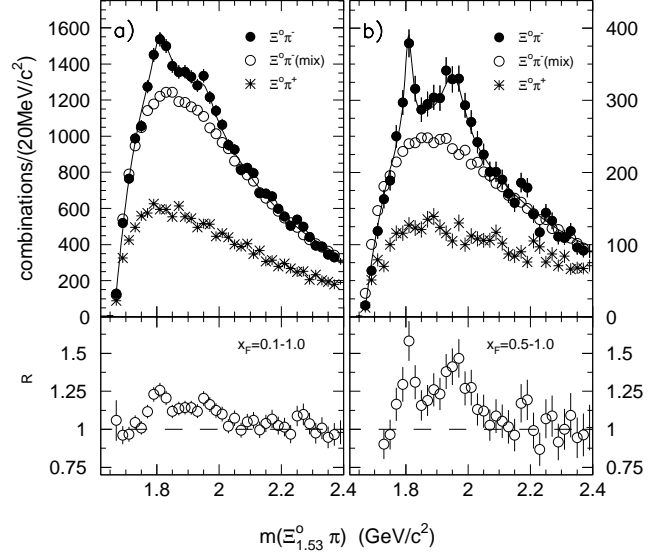


Fig. 2. The $\Xi^- \pi^+ \pi^-$ effective mass distribution in different x_F regions. The open circles show fake events generated by event mixing, the stars represent the background shape from "wrong sign" combinations. The lower parts display the ratio of the observed spectra and the backgrounds from event mixing.

beam track and the production vertex was required to be less than $6 \cdot \sigma$ ($\sigma \approx 25 \mu\text{m}$). This requirement reduced the contributions from neutrons and π^- originating from Σ^- decays upstream of the target. Events were also rejected if the beam track was connected to an outgoing track.

Finally, Ξ_{1530}^0 candidates to be used in the search for $\Xi^- \rightarrow \Xi_{1530}^0 \pi^-$ decays were selected from all combinations of an accepted Ξ^- with a positively charged particle emerging from the production vertex. The reconstructed $\Xi^- \pi^+$ mass had to be within $\pm 10 \text{ MeV}/c^2$ and $\pm 10 \cdot \sigma_m$ of the Ξ_{1530}^0 mass, σ_m being $3.7 \text{ MeV}/c^2$ typically.

4 Observed Ξ_{1530}^0 , Ξ_{1820}^- and Ξ_{1950}^- signals.

Fig. 1 shows the $\Xi^- \pi^+$ mass distribution for all combinations of a Ξ^- candidate with a positive particle from the production vertex. A clear signal of Ξ_{1530}^0 decays is visible. In order to estimate the number of Ξ_{1530}^0 decays, the distribution was fitted by a combination of a Voigtian function (convolution of a Breit-Wigner and a Gauss distribution) with a Legendre polynomial of 3rd order. The width of the underlying Breit-Wigner distribution was fixed to the known value $\Gamma(\Xi_{1530}^0) = 9.1 \text{ MeV}/c^2$ [17]. The position of the signal $M = (1532.2 \pm 0.5) \text{ MeV}/c^2$ is in good agreement with the known value of the Ξ_{1530}^0 mass, $M = (1531.8 \pm 0.3) \text{ MeV}/c^2$ [17]. The mass resolution resulting from the fit in this mass region is $\sigma_{Data} = 3.7 \text{ MeV}/c^2$, slightly higher than the value $\sigma_{MC} = 3.2 \text{ MeV}/c^2$ obtained from a Monte Carlo simulation. The same 15% difference between measured and Monte Carlo

x_F	Copper	Carbon
0.00 - 0.15	6.62 ± 0.65	1.80 ± 0.17
0.15 - 0.30	7.18 ± 0.36	2.00 ± 0.10
0.30 - 0.45	6.56 ± 0.34	2.01 ± 0.09
0.45 - 0.60	4.54 ± 0.24	1.52 ± 0.08
0.60 - 0.75	2.24 ± 0.16	0.93 ± 0.05
0.75 - 0.90	1.46 ± 0.12	0.43 ± 0.03

Table 2. Differential cross section of Ξ_{1530}^0 production by Σ^- in copper and carbon as a function of x_F in mb.

mass resolutions was found for Λ^0 , Ξ^- and Ω^- decays (see Tab. 1).

The $\Xi^- \pi^+ \pi^-$ mass distribution for all combinations of a Ξ_{1530}^0 candidate with a negative particle from the interaction vertex is presented in Fig. 2. The left part of this figure shows the distribution for the range $0.1 < x_F < 1$. An enhancement at 1820 MeV/ c^2 is visible. Fig. 2b is for $x_F > 0.5$. Here the signal at 1820 MeV/ c^2 becomes much clearer and a second wider peak appears at about 1960 MeV/ c^2 .

The subtraction of the background under the signals was done in the following way. We estimated the shape of the background distributions by “event mixing” [18], combining the Ξ^- from one event with all $\pi^+ \pi^-$ pairs from another event. The true and the mixed distributions were normalized to each other in the mass range of 2.1-2.6 GeV/ c^2 . The mixed distributions thus obtained are presented in the upper parts of Fig. 2 by open circles. In the lower panels of Fig. 2 we plot the ratios of the experimental mass distribution to this background distribution. Above 2100 MeV/ c^2 the ratios are consistent with a constant value of one. The effective mass distributions of “wrong” sign combinations $\Xi^- \pi^+ \pi^+$ are indicated by the stars in the upper parts of Fig. 2. They show also no structure in the region of interest and - except for a normalization constant - their shapes are consistent with the mixed distributions.

The resulting mass and width of the Ξ_{1820}^- are $M = (1817 \pm 3)$ MeV/ c^2 and $\Gamma = (23 \pm 13)$ MeV/ c^2 , where the quoted errors are the statistical errors of the fit. The apparatus resolution used was $1.15 \cdot 3.4$ MeV/ $c^2 \approx 3.9$ MeV/ c^2 (see Tab. 1). These values are in good agreement with the world average values $M = (1823 \pm 5)$ MeV/ c^2 and $\Gamma = 24_{-10}^{+15}$ MeV/ c^2 [17].

The mass and width of the second peak are $M = (1955 \pm 6)$ MeV/ c^2 and $\Gamma = (68 \pm 22)$ MeV/ c^2 , respectively. Also these values are in agreement with the average values from the earlier experiments, $M = (1950 \pm 15)$ MeV/ c^2 and $\Gamma = (60 \pm 20)$ MeV/ c^2 [17]. It is, however, not clear whether this signal has its origin in one or several states since several Ξ^* resonances were claimed to be observed in this mass region. In the following, we will treat the second peak as the decay of a single Ξ_{1950} state.

5 Ξ^* production cross sections.

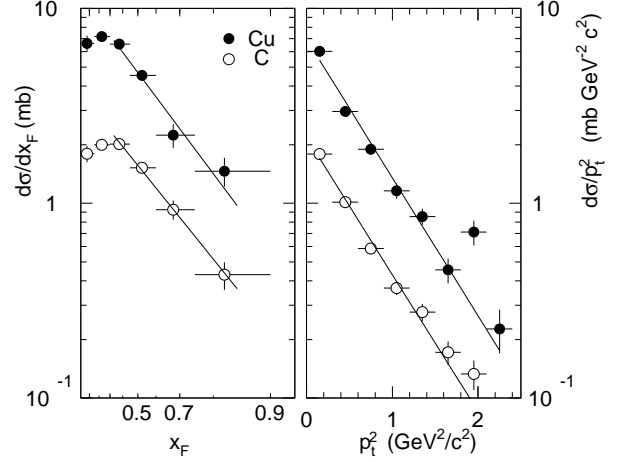


Fig. 3. $d\sigma/dx_F$ [μb] and $d\sigma/dp_t^2$ [$\mu\text{b}/(\text{GeV}/c)^2$] of inclusive Ξ_{1530}^0 production by Σ^- in copper and carbon.

p_t^2	Copper	Carbon
0.00 - 0.30	6.03 ± 0.25	1.79 ± 0.07
0.30 - 0.60	2.96 ± 0.16	1.02 ± 0.05
0.60 - 0.90	1.90 ± 0.13	0.59 ± 0.04
0.90 - 1.20	1.16 ± 0.10	0.37 ± 0.03
1.20 - 1.50	0.86 ± 0.08	0.28 ± 0.03
1.50 - 1.80	0.46 ± 0.07	0.17 ± 0.02
1.80 - 2.10	0.71 ± 0.10	0.13 ± 0.02
2.10 - 2.40	0.23 ± 0.06	—

Table 3. Differential cross section of Ξ_{1530}^0 production by Σ^- in copper and carbon as a function of p_t^2 in mb/(GeV/ c) 2 .

5.1 The Ξ_{1530}^0 production cross section.

The differential cross section as a function of the Feynman variable x_F and the squared transverse momentum p_t^2 , were calculated using the following formula:

$$\sigma(x_F, p_t^2) = \frac{3/2}{BR(\Lambda^0 \rightarrow p\pi^-)} \cdot \frac{N_{\Xi_{1530}} M}{\varepsilon(x_F, p_t^2) N_b \rho l N_A}. \quad (1)$$

Here $N_{\Xi_{1530}}$ is the number of observed Ξ_{1530} in the particular region of the corresponding kinematical variables and ε denotes the overall acceptance including reconstruction and trigger efficiencies. N_b is the number of incoming beam particles tagged as Σ^- , corrected for beam contaminations (see below) and for losses due to the dead time of the trigger and the data acquisition system. M , ρ , l are the atomic mass, the density and the length of the target, respectively; N_A denotes Avogadro’s number. The branching ratio of $\Xi_{1530}^0 \rightarrow \Xi^- \pi^+$ decay is taken to be 2/3, as given by isospin conservation.

The Ξ^- contamination of the tagged beam was measured to be $(1.26 \pm 0.07)\%$ of the Σ^- flux [9]. The production cross section of the Ξ_{1530}^0 by Ξ^- has been measured in a previous hyperon beam experiment [11] and the final

values of our measurement were corrected for this contamination. Typically, this correction amounts to 6%.

About 12% of the tagged beam particles are fast π^- [9]. The cross section of Ξ_{1530}^0 production by pions has not been measured by any previous experiment. In contrast, the production cross section of Ξ^- by pions has been measured in several experiments (see [9] and earlier references therein). From these measurements we derive a 2% contribution from pions to the Ξ^- production in our beam. Assuming the same ratio to holds for Ξ_{1530}^0 production, we subtracted this contribution from the final distributions.

The tagged beam also contains a K^- contamination of 2.1%. The production cross section of Ξ_{1530}^0 by K^- , however, is known only below 16 GeV/c [19]. It decreases slowly in the interval 4.2 - 16 GeV/c. Adopting the maximum value of 43 μb as the production cross section at 345 GeV/c we conclude that at most 0.4% of the observed Ξ_{1530}^0 yield can be attributed to the K^- content of the beam, which is negligible.

The corrected differential production cross sections are shown in Fig. 3 and listed in tables 2 and 3 for copper and carbon targets, respectively. Only fit errors are quoted here. The cross sections were parameterized by a function of the form:

$$\frac{d^2\sigma}{dp_t^2 dx_F} = C(1 - x_F)^n \cdot \exp(-bp_t^2), \quad (2)$$

which is based on quark counting rules and phase space arguments [20]. The three parameters C , n , and b were assumed to be independent of p_t^2 and x_F . The values of n and b obtained from the fits are listed in Tab. 6 for each target, and the fits are shown in the figures as straight lines over the fit range. No significant difference is observed between the values obtained from the copper and the carbon target.

Fig. 4 shows the nuclear mass dependence of Ξ_{1530}^0 production as a function of x_F (top) and p_t^2 (bottom). Also shown are the values observed for Ξ^- production [9]. The left-hand scales give the cross section ratio:

$$R = \frac{\sigma_{Cu}}{\sigma_C} \cdot \frac{A_C}{A_{Cu}} \quad (3)$$

The right-hand scale shows the corresponding values of α in the conventional parametrization for the A dependence:

$$\sigma = \sigma_0 \cdot A^\alpha \quad (4)$$

The dashed lines correspond to $\alpha=2/3$ and $\alpha=1$.

The values for Ξ^- and Ξ_{1530}^0 production are very similar to each other and to those observed in other hadroproduction processes which can be summarized as $\alpha(x_F) = 0.8 - 0.75x_F + 0.45x_F^2$ [21] (solid line in the upper part of Fig. 4). There is no visible dependence of α on p_t^2 .

The total production cross sections per nucleus for copper and carbon are listed in Tab. 6. The quoted errors include an overall systematic error stemming from uncertainties of the efficiency determination (15%), the trigger simulation (10%) and the corrections for beam contaminations (7%). Adding the systematic errors quadratically we estimated the total systematic error to be 20%.

x_F	Ξ_{1820}^-	Ξ_{1950}^-
0.10 - 0.25	30.6 ± 10.8	—
0.25 - 0.40	34.7 ± 7.4	13.8 ± 5.8
0.40 - 0.55	21.4 ± 6.4	4.6 ± 5.2
0.55 - 0.70	15.4 ± 5.1	19.9 ± 5.8
0.70 - 0.85	17.7 ± 3.9	26.2 ± 4.5
0.85 - 1.00	16.9 ± 2.8	16.5 ± 2.8

Table 4. BR $\cdot d\sigma/dx_F$ per nucleon [μb] of inclusive Ξ^* production by Σ^- .

p_t^2	Ξ_{1820}^-	Ξ_{1950}^-
0.00 - 0.30	16.7 ± 4.9	8.1 ± 4.6
0.30 - 0.60	12.4 ± 3.8	6.7 ± 3.7
0.60 - 0.90	14.2 ± 3.6	10.9 ± 3.1
0.90 - 1.20	9.6 ± 2.9	8.6 ± 2.5
1.20 - 1.50	11.4 ± 2.5	6.5 ± 1.9
1.50 - 1.80	4.3 ± 2.2	4.4 ± 2.1
1.80 - 2.10	4.2 ± 1.4	3.8 ± 1.6
2.10 - 2.40	3.6 ± 1.7	2.7 ± 0.9

Table 5. BR $\cdot d\sigma/dp_t^2$ per nucleon [$\mu b / (\text{GeV}/c)^2$] of inclusive Ξ^* production by Σ^- .

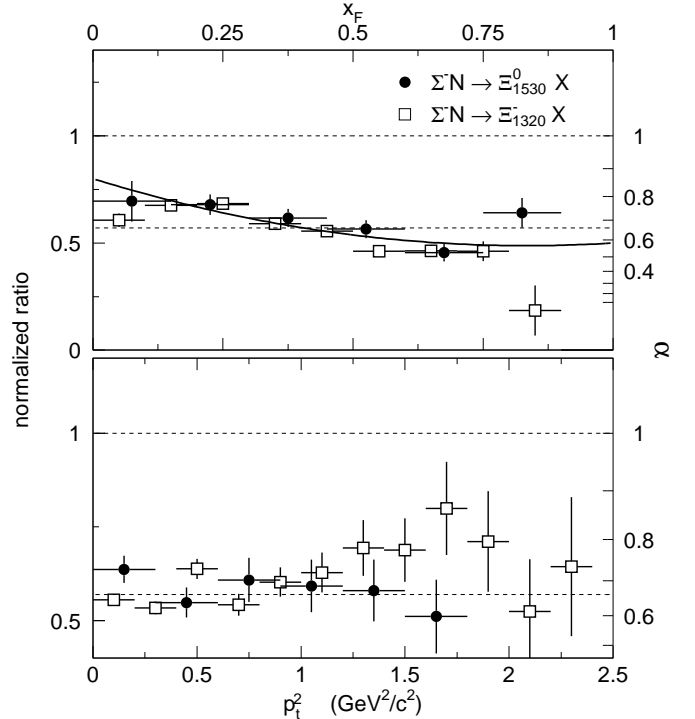


Fig. 4. Normalized ratio R of the copper and carbon cross section (see Eqn. 3) for Ξ_{1530}^0 (dots) and Ξ_{1320}^0 (open squares, ref. [9]) production by Σ^- as a function of x_F (top) and p_t^2 (bottom). The right scale indicates the exponent α in case of an A^α dependence. The solid line in the upper part marks a polynomial fit to a compilation of target attenuation factors given in ref. [21].

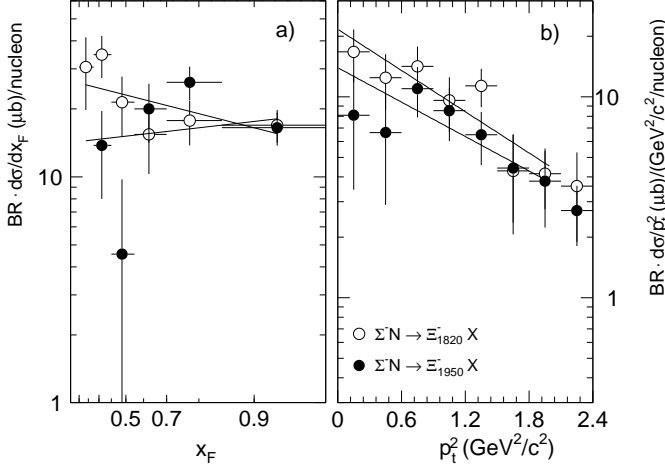


Fig. 5. Differential cross sections times branching ratio per nucleon of inclusive Ξ_{1820}^- and Ξ_{1950}^- production by Σ^- . The lines represent fits to the data according to Eqn. 2

The total production cross section per nucleon for $x_F > 0$ was obtained by extrapolating the differential cross sections measured on Cu and C in each bin of x_F using the values of α obtained in the same bin. The result is $\sigma = (218 \pm 44) \mu b$, where the error is dominated by the systematic error quoted above.

5.2 The Ξ_{1820}^- and Ξ_{1950}^- production cross sections.

The statistics of the observed Ξ_{1820}^- and Ξ_{1950}^- signals is not sufficient to measure the cross section for each target separately. We therefore assume that the inclusive production of these states has the same nuclear dependence as inclusive Ξ^- and Ξ_{1530}^0 production, and analyze the data from the copper and carbon targets together. The differential cross sections are again parameterized by Eqn. 2.

Fig. 5 shows the differential cross section per nucleon multiplied by the branching ratio as a function of x_F and p_t^2 . Only statistical errors are shown. The corresponding numbers are listed in tables 4 and 5. The inclusive production cross section per nucleon, $\sigma \cdot BR$ and the values of the fit parameters n and b are listed in Tab. 6. There are no experimental data on Ξ_{1820} or Ξ_{1950} production by Ξ^- , K^- or π^- . Since, however, the correction to the total Ξ_{1530}^0 production cross section from the beam contaminations amounts to 7% only, we neglect this correction here. A 7% error from the uncertainties of this correction is included in the total systematic error of 20%.

5.3 The Ξ_{1690}^0 production cross section.

In a previous publication [16] we reported a measurement of $\sigma \cdot BR$ for $\Xi_{1690}^0 \rightarrow \Xi^- \pi^+$ production relative to Ξ_{1530}^0 production of

$$\frac{\sigma \cdot BR(\Xi_{1690}^0 \rightarrow \Xi^- \pi^+)}{\sigma \cdot BR(\Xi_{1530}^0 \rightarrow \Xi^- \pi^+)} = 0.022 \pm 0.005.$$

This value corresponds to the observed kinematic range, $0.1 < x_F < 1$, and was extracted by assuming equal x_F and p_t dependence of Ξ_{1690}^0 and Ξ_{1530}^0 production. With our present results we are now able to estimate a possible systematic variation of the production cross section by calculating the ratio of the detection efficiencies of the two states for three different x_F and p_t^2 dependencies of the Ξ_{1690}^0 production cross section, using the measured differential production spectra of the Ξ_{1530}^0 , Ξ_{1820}^- and Ξ_{1950}^- . The values of the parameters n and b used in the MC calculation were taken from Tab. 6.

The resulting inclusive production cross section multiplied by the branching ratio is shown in Tab. 7. The quoted values are for the kinematical range $0 < x_F < 1$, the errors are statistical only. The total systematic error on the scale of the cross sections was estimated to be about 25%. The values obtained range from 2.5 to 6.8 μb .

6 Discussion

In our experiment we observed four excited Ξ hyperons under the same conditions, which gives us a unique possibility to compare their production spectra.

In Fig. 6 we show the invariant cross sections for the observed signals including the ground state Ξ^- [9]. For the Ξ_{1820}^- and Ξ_{1950}^- the values plotted are the cross sections multiplied with the branching ratio to $\Xi_{1530}^0 \pi^-$. A strong leading particle effect is seen for the Ξ states produced. The comparison of the x_F behaviour of the cross sections shows that the octet and decuplet ground states Ξ^- and Ξ_{1530}^0 are produced with similar x_F spectra, with the Ξ_{1530}^0 cross section being smaller by a factor of about 5. The x_F spectra of the excited states Ξ_{1820}^- and Ξ_{1950}^- are significantly harder (see Tab. 6). This nicely illustrates that simple quark counting rules which reflect only the quark flavour contents of the involved baryons (see e.g. [20]) are not able to describe the hyperon production.

The p_t^2 spectra of the Ξ_{1530}^0 shown on the right-hand side of Fig. 3 have an exponential shape throughout the observed kinematical range $0 < p_t^2 < 2.4$ $(\text{GeV}/c)^2$, with slope parameters $b \approx 1.6$ $(\text{GeV}/c)^{-2}$. The p_t^2 spectrum of the Ξ^- has a similar slope with $b \approx 2.0$ $(\text{GeV}/c)^{-2}$ in the range $0 < p_t^2 < 1.0$ $(\text{GeV}/c)^2$, but a much harder p_t^2 spectrum above 1 $(\text{GeV}/c)^2$ corresponding to $b \approx 0.6$ $(\text{GeV}/c)^{-2}$ (see Fig. 5 of [9]). Also the p_t^2 spectra of the Ξ_{1820}^- and Ξ_{1950}^- shown in Fig. 5 are much harder than that of the Ξ_{1530}^0 or the soft part of the Ξ^- spectrum. The slope parameters $b = (0.8 \pm 0.2)$ $(\text{GeV}/c)^{-2}$ for the Ξ_{1820}^- and $b = (0.7 \pm 0.25)$ $(\text{GeV}/c)^{-2}$ for the Ξ_{1950}^- are close to the slope of the Ξ^- distribution above 1 $(\text{GeV}/c)^2$.

Considering this agreement one may speculate whether decays of high lying Ξ^* resonances may contribute to the high- p_t tail of the Ξ^- hyperons. However, taking the decrease of the hyperon mass during the decay chain into account, the apparent slope parameter b for the sequentially produced Ξ^- will increase by typically a factor of $(1820/1320)^2 \approx 2$ to a value of about 1.5 $(\text{GeV}/c)^{-2}$.

Particle	# events	σ [mb] per nucleus	σ [μ b] per nucleon	n	b (GeV/c) $^{-2}$
Ξ_{1320}^- copper carbon		16.72 ± 0.21	1000 ± 40	1.97 ± 0.04	1.90 ± 0.04
		5.40 ± 0.07		2.08 ± 0.04	2.00 ± 0.04
Ξ_{1530}^0 copper carbon	9333 ± 171	4.3 ± 0.9	218 ± 44	1.32 ± 0.08	1.63 ± 0.06
	9547 ± 157	1.30 ± 0.26		1.21 ± 0.07	1.62 ± 0.06
			$\sigma \cdot BR$		
Ξ_{1820}^-	1045 ± 116		21 ± 5	0.2 ± 0.1	0.8 ± 0.20
Ξ_{1950}^-	872 ± 137		12 ± 3	-0.1 ± 0.1	0.7 ± 0.25

Table 6. Number of reconstructed events and total inclusive Ξ^* production cross sections per nucleus and nucleon. n and b are the fit parameters of the differential cross sections with their fit errors (see text). The data for Ξ_{1320}^- were taken from Ref. [9].

x_F spectrum as for	Cross section per nucleon [μ b]
Ξ_{1530}^0	2.5 ± 0.1
Ξ_{1820}^-	5.6 ± 0.2
Ξ_{1950}^-	6.8 ± 0.2

Table 7. $\sigma \cdot BR$ per nucleon of inclusive Ξ_{1690}^0 production for different hypotheses about the x_F spectrum.

Furthermore, the two-step decays

$$\Xi_{1820,1950}^- \rightarrow \Xi_{1530}^0 \pi^- \rightarrow \Xi^- \pi^+ \pi^- \quad (5)$$

contribute not more than 3% to the yield of Ξ^- hyperons at large $p_t^2 > 1$ (GeV/c) 2 . The alternative decay chain $\Xi_{1820,1950}^- \rightarrow \Xi_{1530}^0 \pi^0 \rightarrow \Xi^- \pi^0 \pi^0$ increases this yield by an additional factor 5/4. In Ref. [22] the ratio

$$R = \frac{\Xi_{1820,1950}^- \rightarrow \Xi \pi + \Xi \pi \pi}{\Xi_{1820,1950}^- \rightarrow \Xi_{1530} \pi} \quad (6)$$

is estimated to be 1.5 and 2.8 for Ξ_{1820} and Ξ_{1950} decays, respectively. However, according to later observations [23] which are also consistent with earlier studies [24], the contribution via non-resonant decays $\Xi_{1820}^- \rightarrow \Xi^- \pi^0$ are a factor of 3 lower than the yield resulting from the resonant decay chain given in Eqn. 5. Therefore, we take the values from Ref. [22] as an upper limit and estimate that at most 10 % of the observed Ξ^- hyperons at high p_t are decay products of negative Ξ_{1820}^- or Ξ_{1950}^- resonances. On the other hand, neglecting any non-resonant decays we obtain a lower limit of about 4%. Of course additional higher lying Ξ^* states and particularly neutral Ξ 's will add further contributions. Nonetheless, both the relatively low yield and the expected increase of the slope parameter b in sequential decays make it rather unlikely that sequential decays of high-lying Ξ^* resonances are the main origin of the high- p_t tail of the Ξ^- spectrum.

The large background under the Ξ_{1690}^0 signal does not allow the x_F and p_t spectra to be measured. We expect the observed decay channel $\Xi^- \pi^+$ to be the main decay channel, since the only other possible decay channels, $\Lambda \bar{K}$ and $\Xi_{1530}^0 \pi^0$, have thresholds of 1613 and 1667 MeV/c 2 respectively, and therefore a much smaller phase space than

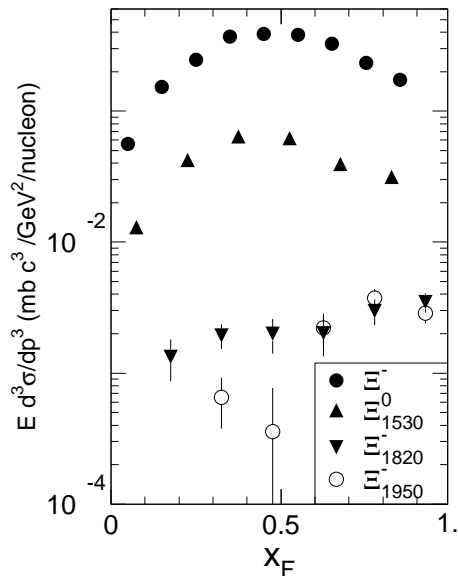


Fig. 6. Invariant cross sections per nucleon of inclusive Ξ^- and Ξ^* production by Σ^- .

the $\Xi^- \pi^+$ channel with its threshold at 1462 MeV/c 2 . Thus we expect the production cross section to be 2–10 μ b per nucleon in the range $0 < x_F < 1$, a factor of 20 or more below the corresponding Ξ_{1530}^0 cross section.

There is only one publication about the branching ratio of $\Xi_{1820}^- \rightarrow \Xi_{1530} \pi$ decay, giving a value 0.3 ± 0.15 [24]. This yields about (70 ± 35) μ b per nucleon for inclusive Ξ_{1820}^- production, which is about a factor of three below the Ξ_{1530}^0 cross section. Nothing is known about the Ξ_{1950}^- decay branching ratios. The measured value of $\sigma \cdot BR = (12 \pm 3)$ μ b for Ξ_{1950}^- production is smaller by a factor of 2 than the corresponding value $\sigma \cdot BR = (21 \pm 5)$ μ b for Ξ_{1820}^- production.

In Fig. 7 we compare our experimental results with theoretical calculations based on PYTHIA [25] and the Quark-Gluon String Model (QGSM, see [26] and references therein).

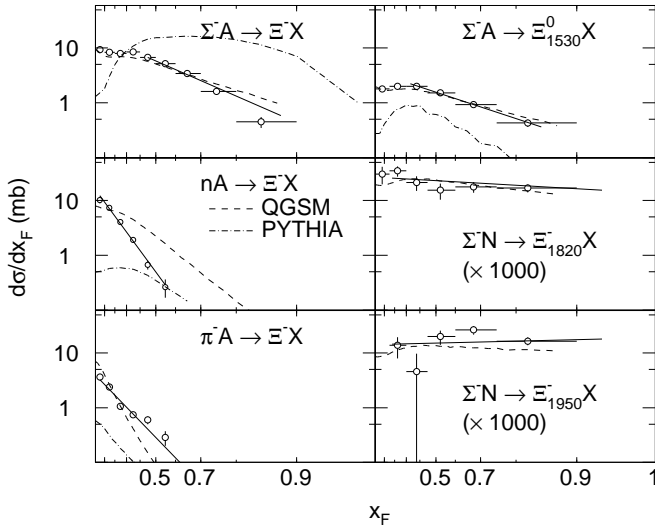


Fig. 7. Comparison of differential cross sections of inclusive Ξ hyperons production with PYTHIA (— · —) and QGSM (— —) predictions. The QGSM cross sections for excited Ξ 's were normalized to measured value. The solid lines represent the fit to the data according to Eqn. 2.

We have used PYTHIA with its default set of parameters, and made no effort to adjust them to better fit the experimental data (for reasons to be explained later). Among the essential details, we only mention the inclusion of elastic and diffraction processes (PYTHIA option MSEL=2) and the usage of the Lund string fragmentation algorithm. The latter is closer to the QGSM ideology than ‘independent’ or ‘cluster’ fragmentation. The striking difference between the calculated cross sections, $\sigma_{\Sigma \rightarrow \Xi}$ versus $\sigma_{n \rightarrow \Xi}$ and $\sigma_{\pi \rightarrow \Xi}$, is due to the hierarchy of probabilities that PYTHIA attributes to the various species of quarks and diquarks appearing from the colour string fragmentation. The creation of a doubly strange diquark ss (which is necessary to produce Ξ 's from π or n) is suppressed relative to the creation of a single strange quark (which is sufficient to form a Ξ from a Σ) by a factor of 30. Such a suppression is also responsible for the relatively low abundance of Ξ at $x_F \simeq 0$ in the case of Σ beams.

Changing PYTHIA's default parameters in order to reach agreement with the data presented here, one would lose the consistency with other experimental results. For example reducing the suppression of doubly strange diquarks with respect to singly strange and non-strange diquarks one would no longer reproduce the cross section ratios observed in $\Xi/\Lambda/p$ inclusive production by protons [4]. A suppression of all diquarks with respect to single quarks would deteriorate the baryon to meson multiplicity ratios [27, 28]. Reducing the probability of single strange quark creation would cause difficulties with K/π and Λ/p ratios in the proton [28] and pion [29] beams.

The Quark-Gluon String Model offers two free parameters (for each isotopic family) that are the absolute probabilities to form the final state baryon via different fragmen-

tation mechanisms. The baryon may be produced either directly from the beam diquark, or indirectly, in a remote part of the colour string (this includes quark, antiquark and antidiquark fragmentation cases). Although the absolute normalization of these two contributions is arbitrary, their x_F behaviour is strictly defined in the model. We have used the normalization freedom to tune the model to the Ξ_{1320} production in Σ^- induced reactions on carbon.

However, the QGSM predicts a stronger leading particle effect in the production of Ξ hyperons by neutrons than observed experimentally [9]. This discrepancy has its origin in the so called ‘baryon junction’ which is introduced in the QGSM. The junction is considered to be as important for the baryon colour structure as the valence quarks themselves. The transmission of a junction from the projectile to a final state baryon creates a strong ‘leading particle effect’ even for a neutron beam, though neutrons have only a single quark in common with Ξ hyperons.

With respect to the production of excited hyperon resonances, we have extended the original QGSM version by introducing a new assumption that the fragmentation into an excited state proceeds by an exchange of a shifted Regge trajectory (e.g., Δ or N^*) rather than by the ordinary nucleon trajectory. Then, the fragmentation functions acquire an extra factor, thus shifting in the same sense the x_F spectra. The absolute normalization of the production cross section still remains a free parameter that cannot be calculated within the theory. With the modification mentioned, the model appears to reproduce qualitatively the different shapes of the observed distributions.

To summarize we have studied the production of several Ξ^* resonances in Σ^- - nucleus collisions at 345 GeV/c. The cross section for inclusive Ξ_{1530}^0 production is about a factor of 5 below that of Ξ_{1320}^- hyperons. The products of cross section and branching ratio for the observed channels $\Xi_{1690}^0 \rightarrow \Xi^- \pi^+$, $\Xi_{1820}^- \rightarrow \Xi_{1530}^0 \pi^-$ and $\Xi_{1950}^- \rightarrow \Xi_{1530}^0 \pi^-$ are lower by yet another order of magnitude. The Ξ_{1820}^- and Ξ_{1950}^- resonances show significantly harder x_F and p_t distributions than Ξ^- and Ξ_{1530}^0 hyperons. A comparison of the measured x_F distributions to PYTHIA and QGSM predictions provides only a partial agreement.

Acknowledgements

It is a pleasure to thank J. Zimmer and G. Konorova for their support in setting up and running the experiment. We are also indebted to the staff of the CERN Omega spectrometer group for their help and support, to the CERN EBS group for their work on the hyperon beam line and to the CERN accelerator group for their continuous efforts to provide good and stable beam conditions. We thank S. Brodsky, B. Kopeliovich and O. Piskounova for helpful discussions.

References

1. J. Badier *et al.*, Phys. Rev. Lett. **39B**, 414 (1972).
2. V. Hungerbühler *et al.*, Phys. Rev. **D12**, 1203 (1975).
3. M. Bourquin *et al.*, Nucl. Phys. **B153**, 13 (1979).
4. M. Bourquin *et al.*, Z. Phys. **C5**, 275 (1980).
5. S.F. Biagi *et al.*, Z. Phys. **C9**, 305 (1981).
6. T.R. Cardello *et al.*, Phys. Rev. **D32**, 1 (1985).
7. S.F. Biagi *et al.*, Z. Phys. **C34**, 187 (1987).
8. BIS-2 Collaboration, A.N. Aleev *et al.*, Sov. J. Nucl. Phys. **44**, 429 (1986).
9. M.I. Adamovich *et al.*, Z. Phys. **C76**, 35 (1997).
10. S.F. Biagi *et al.*, Z. Phys. **C31**, 33 (1986).
11. O. Schneider *et al.*, Z. Phys. **C46**, 341 (1990).
12. T. Tashiro, H. Noda, K. Kinoshita, Z. Phys. **C39**, 499 (1988).
13. A. Dumitru, S.A. Bass, M. Bleicher, H. Stöcker, and W. Greiner, nucl-th/9901046.
14. Yu.A. Alexandrov *et al.*, Nucl. Instr. Meth. A **408**, 359 (1998).
15. W. Beusch, CERN/SPSC/77-70.
16. M.I. Adamovich *et al.*, Eur. Phys. J. **C5**, 621 (1998).
17. C. Caso *et al.*, Eur. Phys. J. **C3**, 1 (1998).
18. G.I. Kopylov, Phys. Lett. **B50**, 472 (1974); D. Drijard *et al.*, Nucl. Instr. Meth. **225**, 367 (1984).
19. M. Baubillier *et al.*, Nucl. Phys. B **192**, 1 (1981).
20. R. Blankenbecler and S.J. Brodsky, Phys. Rev. **D10**, 2973 (1974).
21. W.M. Geist, Nucl. Phys. **A525**, 149c (1991).
22. S. Apsell *et al.*, Phys. Rev. Lett. **24**, 777 (1970).
23. J.B. Gay *et al.*, Phys. Lett. **62B**, 477 (1976).
24. J. Alitti *et al.*, Phys. Rev. Lett. **22**, 79 (1969).
25. T. Sjöstrand, Computer Phys. Comm. **82**, 74 (1994).
26. A.B. Kaidalov and K.A. Ter-Martirosyan, Sov. J. Nucl. Phys. **39**, 1545 (1984); A.I. Veselov, O.I. Piskunova and K.A. Ter-Martirosyan, Phys. Lett. **B158**, 175 (1985); A.B. Kaidalov and O.I. Piskunova, Z. Phys. **C30**, 145 (1986); A.B. Kaidalov, Sov. J. Nucl. Phys. **45**, 1450 (1987); S.P. Baranov, program HIPPOPO, Lebedev Physical Institute preprint 42 (1998).
27. MARK II Collab., M. Piccolo *et al.*, Phys. Rev. Lett. **39**, 1503 (1977); MARK II Collab., G.S. Abrams *et al.*, Phys. Rev. Lett. **44**, 10 (1980).
28. V. Blobel *et al.*, Nucl. Phys. **B69**, 454 (1979); K. Jaeger *et al.*, Phys. Rev. **D11**, 2405 (1975); H. Kishimi *et al.*, Phys. Lett. **B72**, 411 (1978); D. Drijard *et al.*, Z. Phys. **C12**, 217 (1982).
29. A.E. Brenner *et al.*, Phys. Rev. **D26**, 1497 (1982).